



ELSEVIER

Available online at www.sciencedirect.com

SCIENCE @ DIRECT®

Electronic Notes in Discrete Mathematics 20 (2005) 455–474

Electronic Notes in
DISCRETE
MATHEMATICS

www.elsevier.com/locate/ndm

Discrete tomography for reconstruction from limited view angles in non-destructive testing

S. Krimmel^{a,1}, J. Baumann^{b,2}, Z. Kiss^{c,3,4}, A. Kuba^{c,3,4},
A. Nagy^{c,3,4}, and J. Stephan^{b,2}

^a *Physik Department E 21, Technische Universität München, Garching, Germany*

^b *Corporate Technology PS 9, Siemens AG, Munich, Germany*

^c *Dept. of Image Proc. and Computer Graphics, Univ. of Szeged, Szeged, Hungary*

Abstract

We show that discrete tomography (DT) is suitable to increase the possible inspection size of single material oblong objects compared to filtered back projection (FBP) in non-destructive testing (NDT) with 2D X-ray computed tomography (CT). For such objects which are in one dimension larger than the maximum detectable material thickness limited view angles occur and FBP is not suitable for reconstruction. For evaluation of the reconstruction performance a copper phantom (strong absorber) which exhibits typical problems for NDT was manufactured. The increase of the object size with DT reconstruction compared to FBP was estimated to be above 50%.

Keywords: Discrete tomography, limited view angles, sensitivity to distortions, experimental data

¹ Email: xray.external@mchp.siemens.de

² Email: {Joachim.Baumann|Juergen.Stephan}@siemens.com

³ Email: {nagy|kuba|kiss}@inf.u-szeged.hu

⁴ Supported by the OTKA grant T 048476 and NSF grant DMS 0306215.

1 Introduction

The scope of this work is to point out the potential of discrete tomography (DT) for non-destructive testing (NDT) with X-ray computed tomography (CT). A key problem for X-ray CT in NDT is the strong absorption in metal objects. We aim to increase the inspection size of oblong objects which are made of a single material and for which X-ray penetration is limited for a few directions (Fig. 1 a). This is a special case of limited view angle tomography and filtered back projection (FBP) is not suitable as reconstruction method because it requires projection data from all view angles on a circular source trajectory, i.e., usually a 180° scan for parallel beam geometry and a 360° scan for fan beam geometry. If we use FBP despite of the lack of data limited view angle artifacts arise. A compensation is possible with DT using the pre-knowledge about the material composition of the object (As an introduction to DT see [1] and its possible application to NDT is demonstrated in [5]). In addition to this, further pre-knowledge has been implemented with a smoothness penalty term.

Nevertheless, FBP is most popular in NDT because of its high image quality, fast implementation and robustness against distortions in the data, e.g. noise, polychromatic X-rays and scattering. The ultimate goal of this work is the reconstruction of experimental data with DT for which high data quality is crucial. Before starting with the experiments we simulated projection data and analyzed the sensitivity of DT to distortions. For the experiment itself we compared a micro-focus CT system with a Flat Panel Image (FPI) detector at Siemens to a special line detector setup at the EMPA⁵. All investigations were performed with 2D tomography and a special phantom which features relevant NDT tasks like crack and void detection as well as dimensional measuring. A beam hardening correction was performed with a step wedge which was also used to evaluate the system performance. The simulations and experiments were performed by Siemens. The reconstructions with discrete tomography were done at the University of Szeged.

2 The origin of limited view angle artifacts

One useful model to explain the origin of limited view angle artifacts with FBP reconstruction is that limited views are equivalent to missing data in the Fourier space of the object. The central theorem which supports this

⁵ Eidgenössische Materialprüfungs- und Forschungsanstalt, Dübendorf, Switzerland

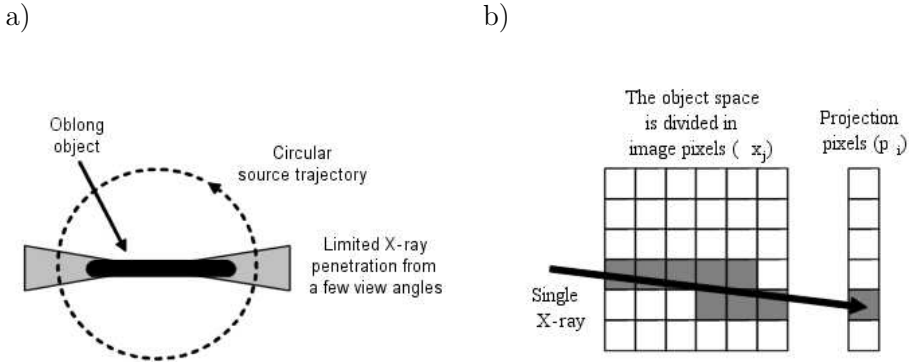


Fig. 1. a) Special case of limited view angle tomography for oblong objects. b) Illustration of one projection equation: It is a projection along a single X-ray onto one detector pixel. The image pixels which contribute to the projection are drawn shaded.

argument is the 2D Fourier slice theorem [2]. It states (for parallel beam geometry) that the 1D Fourier transform of the projection values at a certain angular detector position (line detector) gives the values on a line of the same angular orientation in the 2D Fourier space of the object. It follows that for a 180° turn of the line detector⁶ the Fourier space of the object is completely filled up. In other words, if X-ray penetration is limited from some views this ultimately results in missing data in the Fourier space of the object and thus is equivalent to cutting off some information of the object. It is plausible to assume that this statement is independent of the scanning geometry and the type of reconstruction algorithm.

In contrast to the continuous model given above we can also use an equation system to describe the sampling process for a discrete data set:

$$(1) \quad P = HX \quad \text{or} \quad p_i = \sum_j h_{ij}x_j ,$$

where $H = (h_{ij})$ is called the projection matrix, $X = (x_j)$ is the vector with the reconstructed image pixel values and $P = (p_i)$ is the vector which contains all projection pixel values, i.e., all detector pixel values for all view angles. Each row in this equation system is related to the projection along a single X-ray onto one detector pixel. This is illustrated in Fig. 1 b). The entries of the projection matrix are weight factors which describe the contribution

⁶ Rotating the detector and the source is equivalent to a rotation of the object. In NDT usually the object is rotated.

of the image pixels to the projection pixels. In this model the missing data in Fourier space corresponds to missing equations and an underdetermined equation system. So in general there is more than one possible solution for reconstructing an object from one limited view data set. The solution which is found by filtered back projection can be understood as setting the missing data points in Fourier space to zero. This has been illustrated in [4].

3 Compensation for the lack of data with discrete tomography using pre-knowledge about the object

At this point we might ask how to compensate for the lack of data. In the Fourier picture we can think of associating the unknown to the known points. In the equation system picture this corresponds to adding appropriate equations or to reduce the complexity of the equation system. A practical way of doing this is to use pre-knowledge about the object itself, e.g. material properties, geometric information and smoothness. Discrete tomography is a special kind of tomography that can be applied if the object to be reconstructed consists of a few known homogeneous materials. This information can be included into the reconstruction process giving the possibility to reconstruct such simple objects from a much smaller number of projection values than it is necessary in the case of more complex objects [5]. The objects we want to investigate are single material objects and DT will allow only two values for the reconstructed image pixels: '0' for air and '1' for material. This is the strength of DT but also makes it more sensitive to distortions in the data. It is the central difference to the continuous approach with FBP which can select from all possible absorption values.

Reformulating (1) $HX = P$ as an optimization problem we get the following objective function $C(X)$ to be minimized:

$$(2) \quad C(X) = \|HX - P\|^2 + g \cdot F(X) .$$

The term $g \cdot F(X)$ is an optional penalty term which can control the objective function according to additional prior knowledge about the object to be reconstructed. In our case we have used a special kind of function

$$(3) \quad F(X) = \sum_{i=0}^J \sum_{l \in Q_i^m} g_l \cdot |x_i - x_l| ,$$

where Q_i^m is the set of indices of the $m \times m$ adjacent pixels of the i th lattice pixel. The g_l is the corresponding element of the $m \times m$ Gaussian scalar

matrix, that is,

$$(4) \quad g_l = \frac{1}{2\pi\sigma^2} e^{-(\mu^2+\nu^2)/2\sigma^2} ,$$

where σ is the parameter of the 2D Gaussian function and (μ, ν) is the 2D coordinates of the 1D index l . The g_l scalar weights the differences according to the distance of the i th and l th lattice points. Using this regularization term we can reconstruct objects with big homogeneously connected regions.

In discrete tomography we search a binary vector X which can be calculated by a simulated annealing (SA) combinatorial optimization method. SA is a random-search technique that is based on the physical phenomenon of metal cooling. The system of metal particles gradually reaches the minimum energy level where the metal freezes into a crystalline structure. Based on previous works [3], we first implemented the SA algorithm in the following way (Fig. 2). The algorithm starts from an arbitrary initial binary image $X^{(0)}$, an initial (high) temperature $T^{(0)}$ and calculates the objective function value $C(X)$. Then a position j is randomly chosen in the reconstructed image X . Let X' be the image that differs from X only by changing the value of X in position j to the other binary value, i.e., $x'_j = 1 - x_j$. This change is accepted by the algorithm, i.e., X is replaced by X' if $C(X') < C(X)$. Even if the objective function does not get smaller, the change is accepted with a probability depending on the difference $\Delta C = C(X') - C(X)$.

Formally, the change is accepted even in that case when

$$(5) \quad \exp(-\Delta C/\kappa T) > z ,$$

where κ , T and z are, respectively, the Boltzmann constant ($11.3805 \times 10^{-23} \times m^2 kgs^{-2} K^{-1}$), current temperature, and a randomly generated number from a uniform distribution in the interval $[0, 1]$. Otherwise, the change is rejected, i.e., X does not change in this iteration step. If a change is rejected then we test the level of *efficiency* of changes in the image in the last iterations. It means that we count the number of rejections in the last N_{iter} iterations. If this number is greater than a given threshold value R_{thr} then the efficiency of changes is too low and the SA optimization algorithm will be terminated.

We calculate the variance of the cost function in the last N_{var} iterations. A so-called *equilibrium state* is said to be attained if the present estimate of the current ΔC variance is greater than the previous variance estimate. If the equilibrium state is achieved, we reduce the current temperature (allowing changes with smaller probabilities when the value of the objective function is greater) and let the algorithm run with a lower temperature value (T is replaced by $h \cdot T$, where h is the so-called *cooling factor*). In our experiments

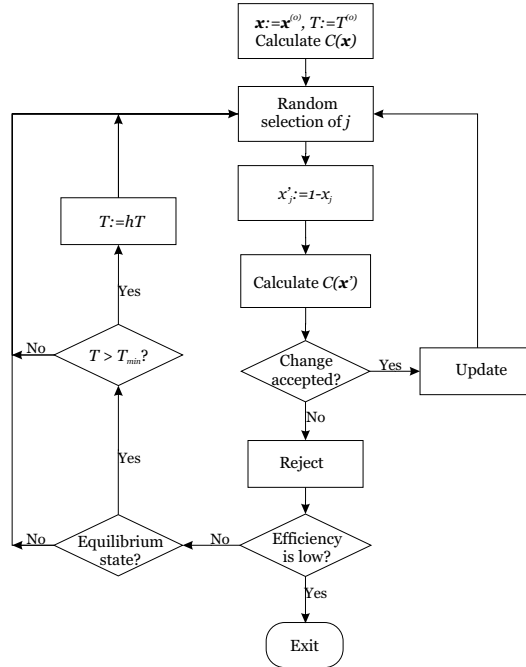


Fig. 2. Flow-chart of the first SA algorithm.

we chose the same value for the parameter as in [6], namely $h = 0.9$.

Finally we implemented the SA as follows. We change all the X vector elements from 0 to 1 or vice-versa in one iteration step. The changes are accepted or rejected similarly like in the previous implementation. When one iteration has been done we reduce the current temperature and start a new iteration step. The algorithm stops when the ratio of the value of the current objective function and the value of the starting objective function fall below a given threshold value ($C(X')/C(X^0) < C_{thr}$) or the current temperature is less than a given temperature ($T < T_{thr}$).

4 Experimental issues

4.1 Investigated objects: Bat phantom and step wedge

We designed a phantom which is a model for a number of non-destructive testing problems. It is made of copper (strong absorber) with gaps (crack detection), drills (void detection), curved and linear shapes (dimensional measuring). Fig. 3 a) shows a photo of the manufactured phantom. This 'bat

phantom' has a cross-sectional size of 70 mm x 16 mm and the smallest drill diameter and gap height are 0.5 mm. The phantom length of 70 mm is a critical size for X-ray penetration in copper at 200 kV. This size was defined with the help of simulated data for different conditions (object size, voltage, dynamic range).

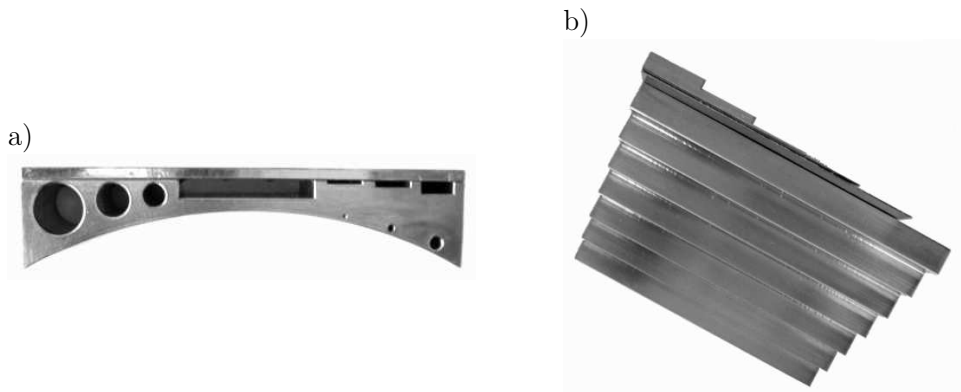


Fig. 3. Photos of the investigated objects. *a)* Bat phantom (cross section 70 mm x 16 mm). *b)* Step wedge (steps from 0 mm to 77 mm).

In addition to the bat phantom we also manufactured a special step wedge of copper (Fig. 3 b). It was designed for two purposes. One was to characterize the dynamic properties and the data quality of the X-ray systems and the other was to obtain a calibration curve for a beam hardening correction. Important features are that it covers the whole range of material thickness occurring in the bat phantom, it has a fine grading and sufficiently large step areas for averaging. This was achieved by arranging the steps in two dimensions, i.e., a coarse grading in the first direction (0 mm to 70 mm in steps of 10 mm) and a fine grading in the second direction (0, 0.5, 1, 2, 4 and 7 mm). In practice two separate step wedges were mounted with perpendicular step orientation to the backside of each other.

4.2 Selecting an appropriate experimental setup to avoid scattering and to achieve a high dynamic range

Experimental measurements were done at two different setups for computed tomography (CT). One is a 225 kV micro-focus system with a 2D Flat Panel Image detector (FPI) at Siemens CT PS9. The other is a 450 kV mini-focus X-ray tube with a 1D line detector at the EMPA. The principle configuration of the two systems is sketched in Fig. 4. The 225 kV micro-focus system is de-

signed for high resolution 3D cone beam computed tomography of small parts. The object is usually magnified by a large factor and the spatial resolution is defined by the focal spot size of the X-ray tube (typ. \varnothing 1-100 μm). At the same time the tube power is limited (typ. < 100 W) and the acquisition time for one projection is rather large. A 2D area detector is necessary to achieve reasonable scanning times in 3D micro-focus CT. The advantages of our FPI detector are a high spatial resolution (in our case 2048 x 2048 pixels of 0.2 mm pixel size) and good noise properties. A disadvantage is that strong internal scattering affects the image quality if large and strong absorbing objects are investigated at higher energies, e.g. the bat phantom at 200 kV. This is a commonly known problem for Flat Panel Image detectors in NDT [7] and the usable dynamic range (maximum detectable intensity / minimum detectable intensity) is significantly reduced for such experiments. Scattering from the object plays a minor role for this setup because the object detector distance is quite large (0.5-1 m).

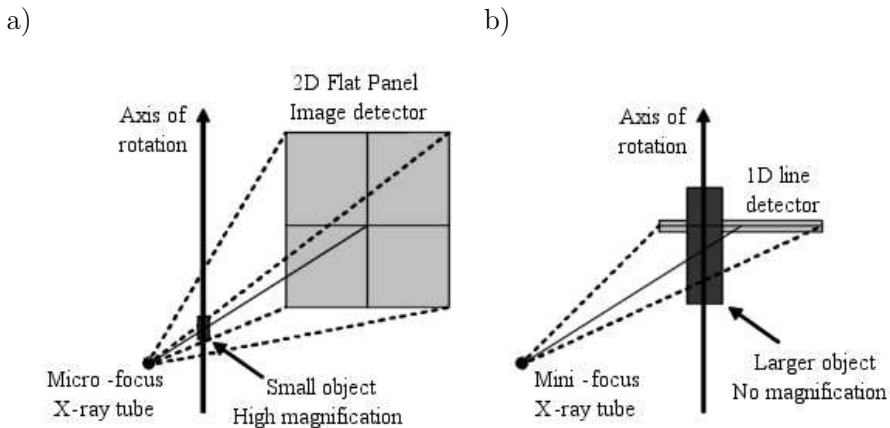


Fig. 4. Geometric configuration of the investigated CT systems. *a)* Micro-focus CT with Flat Panel Image detector and *b)* Mini-focus CT with line detector.

The 450 kV mini-focus system uses 2D fan beam geometry and a line detector with equiangular spaced pixels (Fig. 5). It is designed for the inspection of larger parts with a lower resolution. To enhance penetration possibilities voltages up to 450 kV can be used. A high tube power (1 kW) allows reasonably fast scanning but the focal spot size is large (\varnothing 2.5 mm). If the investigated object is not magnified (or a small magnification is used) the spatial resolution is determined by the detector pixel size. As the detector pixel spacing (2.1 mm) is large and the number of detector channels (125) is small, sub-positions

are scanned to achieve a resolution of 0.1-1 mm. For our experiments an acquisition mode has been used which yielded parallel beam projection data⁷ with 0.23 mm resolution. The most important advantage of the EMPA system is its special line detector which avoids X-ray scattering. It has a tungsten collimator to suppress scattering coming from the object (important because of a small object detector distance). Moreover it uses large and strong absorbing scintillator cells (6 mm $CdWO_4$) such that almost no radiation can pass into the detector housing and cause internal scattering. Therefore the data are not distorted which is a prerequisite for DT reconstruction. Furthermore the usable dynamic range and the possible material thickness for inspection are much larger compared to the FPI detector.

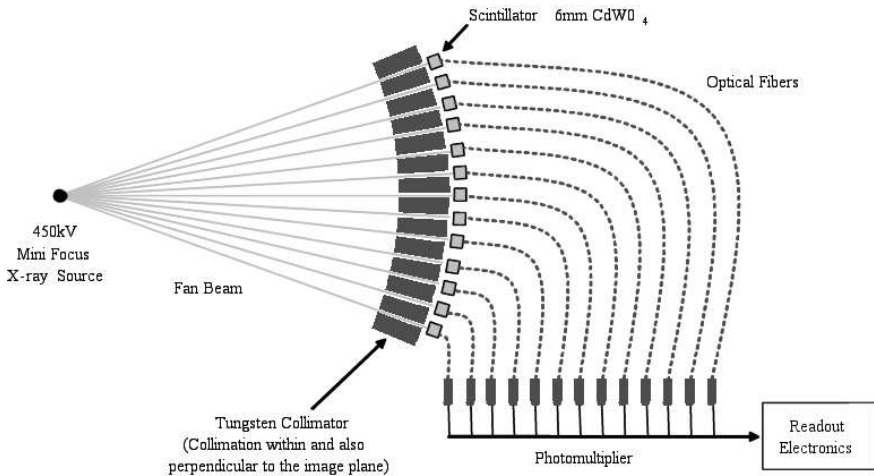


Fig. 5. Schematic of EMPA setup. Scattering is avoided by a special line detector.

4.3 Polychromatic X-rays and beam hardening correction

Polychromatic X-rays cause systematic distortions in the projection data. The reconstructions with FBP and DT rely on line integrals

$$(6) \quad L = \int_{ray} \mu(x, y) ds ,$$

⁷ This is possible by a translational movement of the object parallel to the detector, rotation by the fan angle and re-sorting of the projection rays.

which are computed from the projection data by the logarithmic intensity attenuation

$$(7) \quad L = \ln \left(\frac{I_0}{I_{ray}} \right),$$

where $\mu(x, y)$ is an arbitrary density distribution, I_0 is the free ray intensity and I_{ray} denotes the intensity of a ray after passing the object. This is exact for monochromatic X-rays for which the intensity attenuation is given by the exponential law $I_{ray} = I_0 \exp(-L)$. For polychromatic X-rays the exponential law is additionally integrated over the spectrum. The inversion is not possible and (7) is used as an approximation. In FBP this causes well known beam hardening artifacts.

The term beam hardening is related to the fact that the spectrum is deformed and the mean energy increases when polychromatic X-rays pass through material. Usually a beam hardening filter, i.e., a thin metal plate is used to improve image quality. Fig. 6 a) shows the effect of such a filter on the spectrum.

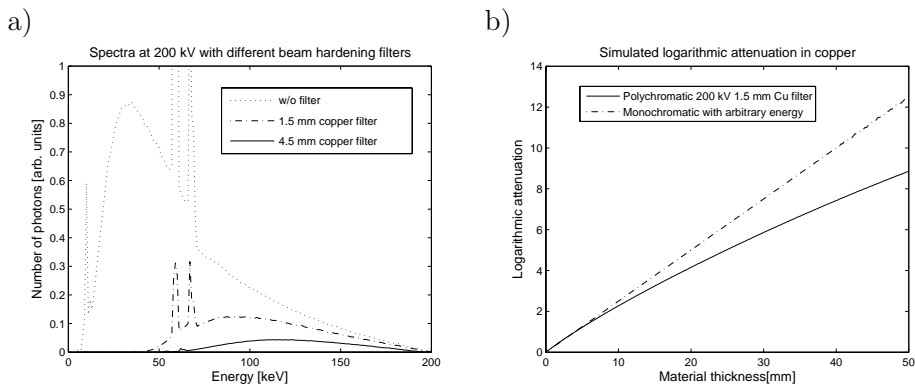


Fig. 6. a) Spectra at 200 kV for different beam hardening filters. b) Logarithmic attenuation in copper for polychromatic and monochromatic X-rays.

For single material objects a beam hardening correction can be performed by pre-processing the projection data. This is done by mapping the measured polychromatic projection values to the correct monochromatic values. In order to do this a calibration curve must be determined with a separate measurement of a step wedge of the same material. Fig. 6 b) shows the simulated logarithmic attenuation in copper for polychromatic and monochromatic X-rays. The ideal monochromatic values are given by a linear function where the slope (energy) can be chosen arbitrarily. Assume that the simulated polychromatic

curve would be a calibration curve for the experiment, i.e., the values on the curve correspond to values that were measured with a step wedge. Then each projection value of the object corresponds to one point on this curve and thus the correct monochromatic value is also known. For the real experiment a simulated calibration curve was fitted to the measured points from the step wedge.

5 Results

5.1 Simulation results

To analyze the performance of discrete tomography we used simulated projection data. We started with ideal monochromatic data and then investigated how noise and polychromatic X-rays affect the reconstruction. Scattering has not been considered in the simulations. The simulation was done for ideal fan beam geometry, i.e., a point source and a linear detector (400 detector pixels, 360 projections in 360° , image pixel size for reconstruction 0.32 mm). The detected intensities were computed by line integrals and the exponential absorption law. Using floating point arithmetics the dynamic range was infinite at first, i.e., no limited views occurred. In order to produce limited views we reduced the dynamic range by setting all values below a certain threshold to this minimum value. For all monochromatic examples the energy was 160 keV. For the polychromatic case a linearly approximated tube spectrum at 160 kV was used with an additional beam hardening filter of 1.5 mm copper. This approximation is sufficient here because the spectrum is not too different from a real one and we look at the problem from a qualitative point of view.

The reconstructions were performed with filtered back projection (FBP) and discrete tomography (DT). On a 2 GHz CPU FBP needed 5 sec. This compares to 10 min for one DT reconstruction (10^5 iterations). Furthermore the DT reconstructions were repeated 50 times and averaged to give a better and more stable result (repeated reconstructions do not give identical results with DT). The total reconstruction time for 50 repetitions was 8h. As an additional feature a smoothness penalty term (Section 3) has been used. Different settings will be mentioned explicitly.

5.1.1 Simulation for the ideal case

The first result we show is for the ideal case, i.e., monochromatic data, no noise and infinite dynamic range. In Fig. 7 the FBP reconstruction for a high sampling with 800 detector pixels and 2880 projections is shown. No artifacts

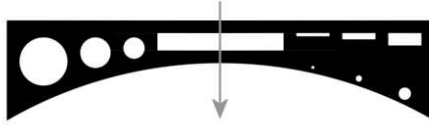


Fig. 7. FBP reconstruction for ideal case with high sampling. The arrow indicates the position where line profiles will be taken.

are visible in this image and we can take it as a reference for comparison with the other results. To point out deviations between different reconstructions we will frequently use vertical line profiles across the most critical region of the bat phantom as indicated by the arrow.

For the investigation with DT we used a low sampling of 400 detector pixels and 360 projections. This optimized the reconstruction time and for DT it is expected to produce no errors (DT is also suitable to reconstruct objects from a very few number of projections). The reconstructions from low sampling with FBP and DT are comparable (Fig. 8 a and b). A closer look at the vertical line profiles (Fig. 8 c and d), reveals ripples (aliasing artifacts) for FBP due to the low sampling but the geometric shape does not change.

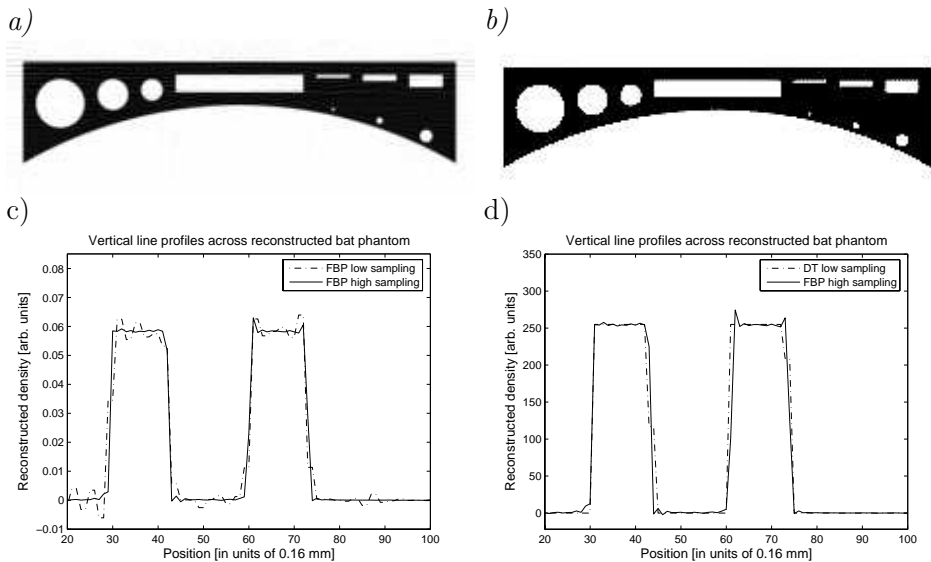


Fig. 8. *a)* FBP and *b)* DT (no smoothness penalty term) reconstruction for the ideal case (with low sampling). The corresponding vertical line profiles are shown in *c)* and *d)*. They are compared to FBP with high sampling.

The profiles are compared to FBP with high sampling for which only some minor spikes are remaining (the sampling is still not high enough). The DT result is exact within the pixel resolution. This result was computed without smoothness penalty term. A smoothness penalty term did not change anything here. Note that the line profiles for the low sampling were re-sampled to match the high sampling case.

5.1.2 Simulation with reduced dynamic range

To simulate a real detector we reduced the dynamic range to 8.5 bit which was found in first experiments. Fig. 9 a) shows the formation of limited view angle artifacts for FBP reconstruction. The amount of artifacts is quite large here and the problem can be seen as difficult to solve. For discrete tomography we tested reconstructions with different options. Fig. 9 b) shows the DT result for one single reconstruction without repetition. Branches have grown wrongly in the critical region. Doing 50 repetitions and averaging (Fig. 9 c) does not help solving the problem. The critical region is smeared out now. The explanation is that DT produces for each repetition a slightly different result, i.e., varying branches. This is due to the statistic nature of the algorithm. In general, the branches do not necessarily appear with DT and limited view angles. In other examples this was not observed. Here the object breaks up because the amount of missing data was too large. In this case a solution could be found only with the help of a smoothness penalty term (Fig. 9 d). The implementation of the smoothness penalty term was a major success of our work. It is not only suitable to suppress branches but also reduces the sensitivity to other

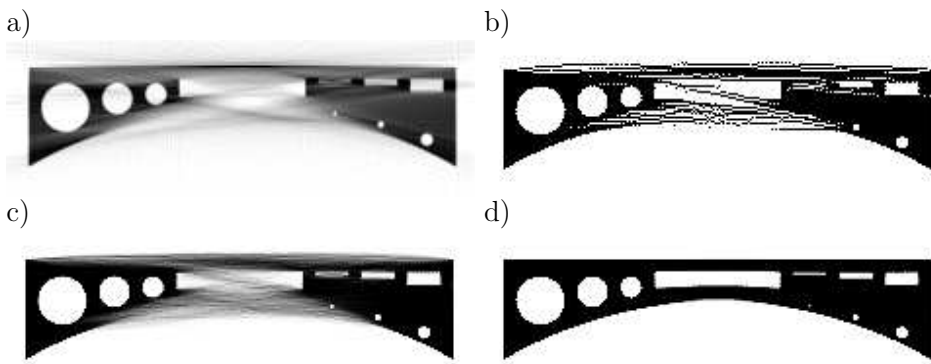


Fig. 9. Reconstructions for 8.5 bit reduced dynamic range. *a)* FBP, *b)* DT (no repetition, no smoothness penalty term), *c)* DT (50 repetitions, no smoothness penalty term) and *d)* DT (50 repetitions, with smoothness penalty term).

distortions, e.g. noise. The overall stability of the algorithm was significantly enhanced.

Comparing the vertical line profile of this result (with smoothness penalty term) to the ideal case with infinite dynamic range (Fig. 10 a), we observe some remaining deviations of the object shape. Here the limits for reduced data can be seen. The maximum penetration length for X-rays in copper at 160 keV and 8.5 bit dynamic is 32 mm. This is also the maximum object length for which FBP reconstruction is exact. Considering that the investigated object length was 70 mm the DT result is quite impressive. This proves that DT is suitable to increase the possible object length for inspection.

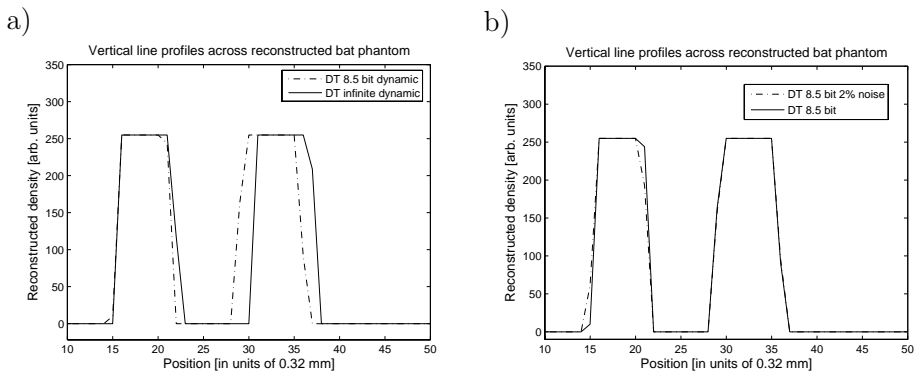


Fig. 10. Vertical line profiles for DT reconstructions. *a)* 8.5 bit reduced dynamic range compared to infinite dynamic range. *b)* 2% noise compared to no noise for 8.5 bit reduced dynamic range.

5.1.3 Simulation with noise and reduced dynamic range

In Fig. 11 we show the impact of 2% (relative to the free ray intensity) quantum noise which was added to the projection data in the case of 8.5 bit reduced dynamic range. An impression for the amount of noise can be obtained from

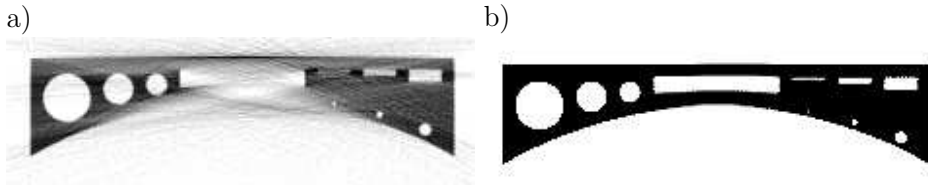


Fig. 11. *a)* FBP and *b)* DT reconstruction from noisy data (2% noise added to the case of 8.5 bit reduced dynamic range).

the FBP reconstruction (Fig. 11 a). The DT reconstruction (Fig. 11 b), is almost unchanged compared to the case without noise. This is clearly visible in the vertical line profile (Fig. 10 b). Only for larger noise levels, e.g. 5% we observed deformations and distortions of the object (not shown). The stability against moderate noise is an important capability considering experimental data. An explanation may be that the distortions are statistically distributed and the correct object is still the best fit to the projection data.

5.1.4 Simulation with polychromatic X-rays and infinite dynamic range

Now we will look at polychromatic data with no noise and infinite dynamic range (no limited view angles). The DT reconstruction (Fig. 12 b) shows significant deviations of the object shape while FBP (Fig. 12 a) reconstructs false grey values inside the object but the object shape does not change. This is clearly seen in the vertical line profiles (Fig. 12 c and d) where the two cases are compared to monochromatic data. We conclude that for experimental data a beam hardening correction is necessary. The shape deformations with DT may be explained by the fact that the distortions for polychromatic X-rays are

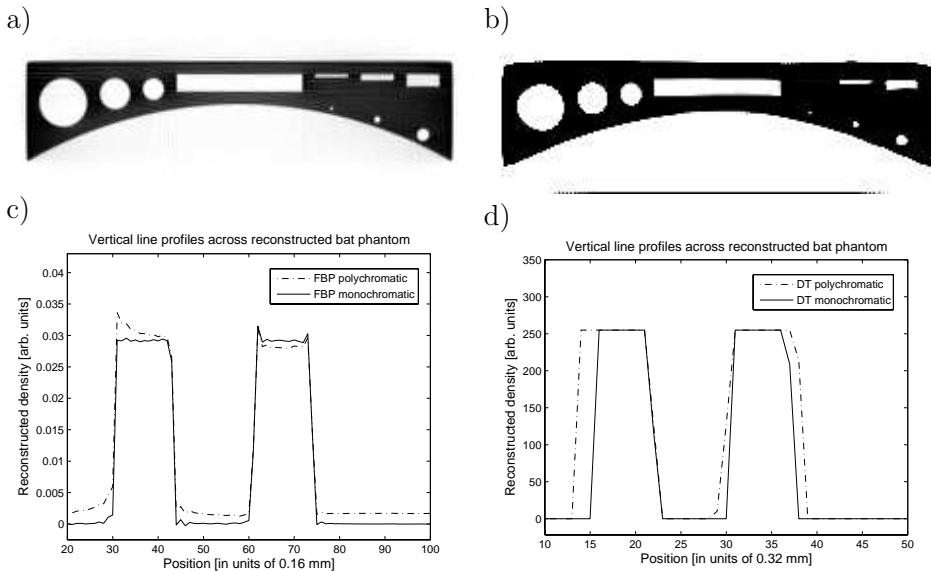


Fig. 12. a) FBP and b) DT reconstruction for polychromatic data (no noise, infinite dynamic range). The corresponding vertical line profiles are shown in c) and d). They are compared to the monochromatic cases (infinite dynamic range). (Note: for FBP high sampling was used for the profiles).

systematical and not statistical as they were for noise. As DT allows only two possible values for the reconstructed image pixels the distortions cannot go anywhere else but to shape deformations. In contrast to this FBP can select from a continuous range of values.

5.2 Experimental results

From the simulation studies we found that a beam hardening correction is necessary for good reconstructions with DT. Furthermore we can expect that also scattering is very critical because it is a systematic distortion as well as polychromatic X-rays are. The measurements were taken with two different setups (Section 4.2). One was at Siemens (micro-focus X-ray tube and FPI detector) and the other at the EMPA (mini-focus X-ray tube and special line detector). If not explicitly mentioned we used 200 kV and a 1.5 mm Cu filter for our experiments. The acquired data were down-sampled for reconstruction: EMPA (parallel beam geometry, 330 detector pixels, 312 projections in 180° , image pixel size for reconstruction 0.23 mm) and Siemens (fan beam geometry, 400 detector pixels, 360 projections in 360° , image pixel size for reconstruction 0.23 mm). The DT reconstructions were performed as described for the simulation part.

5.2.1 Step wedge measurements

For both systems we analyzed the data quality with the help of radiographic images of the step wedge. In Fig. 13 we show selected line profiles across the fine grading at large step thicknesses. With the EMPA line detector the steps

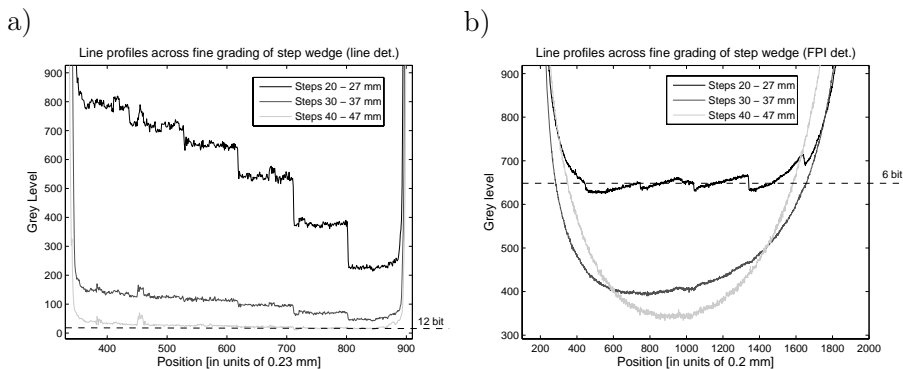


Fig. 13. Line profiles across fine grading of step wedge at large step thicknesses (200 kV): *a)* line detector and *b)* FPI detector.

can be clearly resolved up to 37 mm and a decline of intensity is visible up to 47 mm. This corresponds to a dynamic range of 10 - 12 bit. In contrast to this the dynamic range is significantly reduced for the FPI detector. This can be seen as the line profiles for large step thicknesses are strongly distorted due to scattering inside the FPI detector (Section 4.2). An important remark is that this is only relevant for experiments with strong absorbers and high energies, i.e. the line profiles for the small step thicknesses were not affected (not shown).

The calibration curve for a beam hardening correction (Section 4.3) was determined by fitting simulated curves to the points which were measured with the step wedge. In Fig. 17 a) the measured and corresponding fitted simulated points are plotted for the EMPA line detector. The fit was good and the relative deviation of the two was mostly smaller than 1% for step thicknesses below the maximum penetration length (37 - 47 mm). For the FPI detector the beam hardening effects were dominated by the internal scattering and a beam hardening correction was not practicable.

5.2.2 Reconstruction results for experimental data

At first we will show the reconstruction results for the FPI detector. From the discussion above we expect a strong impact due to the massive scattering effects. For FBP (Fig. 14 a) we observe huge limited view angle artifacts and a strong smearing in the reconstructed image. With continuously increasing distortions the quality of the FBP result decreases continuously. This kind of stability is a major strength of FBP. The behavior of DT is different. Due to the large amount of distortions the reconstruction with DT is not possible any longer (Fig. 14 b). The object 'breaks up' at some level of distortions. A beam hardening correction was not feasible here (Section 5.2.1).

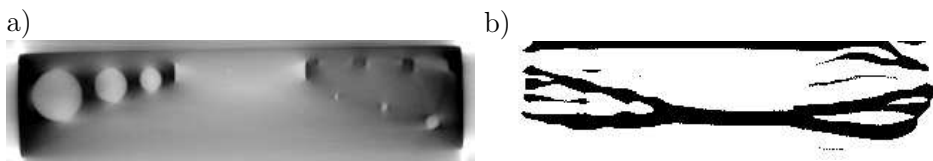


Fig. 14. Attempt to reconstruct data from Flat Panel Image detector (200 kV) with a) FBP and b) DT.

For the EMPA line detector the data quality is much better. With FBP reconstruction of the raw data we observed only very small limited view angle artifacts (not shown). To make the problem a bit more challenging we reduced the dynamic range in a preprocessing step to 10 bit. In a second

pre-processing step the beam hardening correction which was described in sections 4.3 and 5.2.1 was done. The FBP result is shown in Fig. 15 a). Now the reconstruction with DT is also possible (Fig. 15 b). Up to this point all experiments were performed at 200 kV. Another way to solve the problem is to increase the voltage. At 450 kV the limited view angle artifacts in FBP disappeared almost completely (Fig. 16).

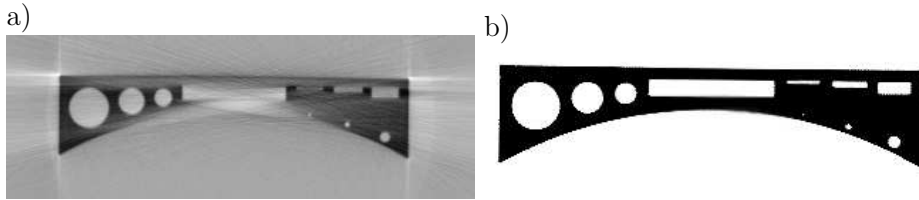


Fig. 15. a) FBP and b) DT reconstruction with beam hardening correction for line detector (200 kV).



Fig. 16. FBP reconstruction with beam hardening correction for line detector (450 kV, high sampling).

For a precise analysis we compared the vertical line profiles of the DT result at 200 kV to the FBP result at 450 kV (Fig. 17 b). The positions of the profiles relative to the object were the same as in the simulation part and were indicated in Fig. 8. Considering the shape of the reconstructed object we found that DT (200 kV) and FBP (450 kV) are in good agreement. A closer look reveals that the FBP case is not perfect because the X-ray penetration is still not fully possible and some artifacts remain in the reconstructed image. The upper center bar is brighter in the image and the corresponding first peak in the vertical line profile is widened a little bit. The geometric shape for the DT reconstruction appears to be quite good. The full width half maximum of the peaks in the vertical profile is 2 mm for the first peak and 2.1 mm for the second peak compared to 2.1 mm in the original object. As the spatial resolution was only 0.23 mm the accuracy was not very high at this stage. This might also be the reason why the smallest drill hole appears slightly too small here. The final result clearly shows that DT can be applied in experiments with high data quality to increase the possible inspection size of

oblong objects. To quantize the improvement the object size (70 mm) can be compared to the penetration limit (37 mm). But FBP may also be suitable to reconstruct objects which are a bit larger than 37 mm because small artifacts may be tolerated. We estimate that the improvement in object size of DT compared to FBP was above 50%.

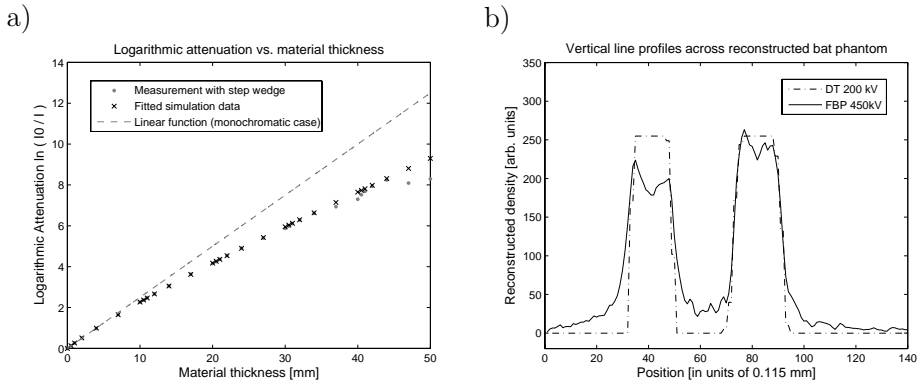


Fig. 17. Plots for line detector: *a)* Beam hardening calibration with step wedge (200 kV) and *b)* Comparison of vertical line profiles for DT (200 kV) and FBP (450 kV, high sampling) reconstructions.

6 Conclusion

We proved that DT is suitable to increase the possible object size of oblong single material objects. The dimensions for the bat phantom were chosen according to similar NDT problems which are difficult to solve. With simulations the limits for DT reconstruction were analyzed. For the best results the implementation of a smoothness penalty term was an important step. Adding moderate noise of 2% did not change the result but polychromatic X-rays caused deviations of the object shape. We concluded that a beam hardening correction is necessary for experimental data. In the experimental part we investigated a micro-focus CT system with a Flat Panel Image (FPI) detector at Siemens and a mini-focus CT system with a special line detector at the EMPA. The EMPA line detector very efficiently avoids scattering and acquires high quality data while the data of the FPI detector is strongly distorted by scattering for this type of experiment (large and strong absorber at high energy). The step wedge was well suited to analyze the performance of the two systems and to determine the calibration curve for a beam hardening

correction. As expected DT reconstruction was not possible for the FPI detector data. In contrast to this the EMPA system delivered good results. The estimated improvement in object size compared to FBP was estimated to be above 50%.

7 Acknowledgements

Thanks to P. Böni and B. Schillinger who are my advisors at the Technische Universität München, A. Flisch for supporting our measurements at the EMPA and M. Goldammer for perusal of the manuscript.

References

- [1] Herman, G. T., and A. Kuba (Eds.), *Discrete Tomography: Foundations, Algorithms, and Applications*, Birkhäuser, Boston, MA, 1999.
- [2] Kak, A.C., and M. Slaney, *Principles of computerized tomographic imaging*, IEEE Press, New York, 1987.
- [3] Kirkpatrick S., C. D. Gelatt, and M. P. Vecchi, *Optimization by simulated annealing*, *Science* **220** (1983), 671–680.
- [4] Krimmel S., J. Stephan, and J. Baumann, *3D computed tomography using a microfocus X-ray source: Analysis of artifact formation in the reconstructed images using simulated as well as experimental projection data*, *Nuclear Instr. and Methods in Physics Research A* **542** (2005), 399–407.
- [5] Kuba A., L. Ruskó, L. Rodek, and Z. Kiss, *Preliminary studies of discrete tomography in neutron imaging*, *IEEE Trans. on Nuclear Science* **52** (2005), 380–385.
- [6] Robert, N., F. Peyrin, and M. J. Yaffe, *Binary vascular reconstruction from a limited number of cone beam projections*, *Med. Phys.* **21** (1994), 1839–1851.
- [7] Zscherpel U., K. Osterloh, and U. Ewert, *Unschärfeprobleme beim Einsatz digitaler Detektoren in der Durchstrahlungsprüfung*, DGZfP Annual Meeting, 2003. With associated web site
<http://www.ndt.net/article/dgzfp03/papers/v22/v22.htm>.